Influence of Modeling and Blade Parameters on the Aeroelastic Stability of a Cantilevered Rotor

Peretz Friedmann*
University of California, Los Angeles, Los Angeles, Calif.

A set of equations describing the coupled flap-lag-torsional dynamics of a cantilevered rotor blade in hover is presented. This set of equations is used to evaluate the influence of structural damping, preconing, and offsets on the linearized aeroelastic stability of some representative blade configurations. The sensitivity of the stability boundaries to the assumptions of approximate linear vs exact nonlinear static blade equilibrium position is considered. Finally, results with the distributed torsional representation of blade properties are compared with those obtained when the root torsional model is used.

Nomenclature

a = two-dimensional lift curve slope
$\bar{A}$, $\bar{B}$ = tip loss coefficients
B_1, B_2 = section constants defined in Appendix A
$\bar{B}^i$ = generalized masses defined in Appendix A
b = half-chord, nondimensionalized with respect to R
C_i = element of matrix $\{C\}$
C_{d0} = profile-drag coefficient
E = Young's modulus of elasticity
E_{c1}, E_{c2}, E_{c3} = terms associated with elastic coupling, defined in Appendix A
$\bar{E}^s$, $\bar{E}^c$, $\bar{E}^{cs}$, $\bar{\bar{E}}^{cs}$ = terms associated with the elastic coupling effect described in Appendix A
$\bar{E}^2 \ldots \bar{E}^8$ = terms associated with elastic coupling, defined in Appendix A
e_A = distance between centroid of tensile member and elastic axis
e_1 = blade pitch bearing offset defined in Fig. 1
F^i, F^i_ϕ, F^i_θ = flap coefficients defined in Appendix A
F_g, $F_{dh}, \ldots F_f$ = flutter derivatives associated with the flap equation, defined in Appendix B
f_1 = generalized coordinate, first coupled root torsional mode
f_1° = static value of f_1 in hover
Δf_1 = perturbation in f_1 about f_1°
g_1 = generalized coordinate, first normal flap mode
g_1° = static value of g_1 in hover
Δg_1 = perturbation in g_1 about g_1°
$\bar{g}_{D1}$, $\bar{g}_{D2}$, $\bar{g}_{D3}$ = equivalent damping terms, defined in Appendix B
G = shear modulus of elasticity
g_{SL}, g_{SF} = dimensional structural damping, in flap and lag, respectively
h_1 = generalized coordinate, first normal inplane mode
h_1° = static value of h_1 in hover
Δh_1 = perturbation in h_1 about h_1°
I_b = mass moment of inertia of elastic part of the blade about its root
$I_{\phi 1}$ = generalized mass of first root torsional mode
i, j, k = unit vectors in x, y, and z directions, Fig. 1
L_{Y2}, L_{Z2} = aerodynamic loads per unit length in the J_2 and K_2 directions
I_2, J_2, K_2; I_3, J_3, K_3 = unit vectors defining deformed blade geometry, shown in Figs. 1b, and 2. J_2 is parallel to hub plane, I_2 and I_3 are tangential to the deformed blade elastic axis
J = torsional stiffness constant
k_A = polar radius of gyration of cross-sectional area effective in carrying tensile stresses about the elastic axis
k_ϕ = root torsional spring constant, control system stiffness
k_0 = polar radius of gyration of cross-sectional mass about its center of gravity
ℓ = length of blade capable of elastic deformation
$L^i, L^i_\theta, L^i_\phi \ldots$etc. = lag coefficients defined in Appendix A
$L_{dg}, \ldots, L_f$ = flutter derivatives associated with the lag equation, defined in Appendix B
m = mass of blade/unit length
$\bar{M}_{F1}, \bar{M}_{L1}, \bar{M}_{\phi 1}$ = generalized mass for the first flap, lag and torsional mode, respectively; defined in Appendix A
$(\bar{M}_\eta)_{111}$, $(\bar{M}_\gamma)_{111}$ = defined in Appendix A
$\bar{P}_{111}$ = described in Appendix A
p_x, p_y, p_z = resultant total loading per unit length in the x, y, and z directions, respectively, subscript I denotes inertia part and A denotes aerodynamic part
q_x, q_y, q_z = distributed torques in the x, y, and z directions, respectively
R = blade radius
S_{ij} = elements of a matrix associated with the calculation of the approximate linear static equilibrium position of the blade
t = time
T^i, T^i_ϕ, $T^i_\theta \ldots$etc. = torsional coefficients defined in Appendix A

Presented as Paper 75-780 at the AIAA/ASME 16th Structures, Structural Dynamics, and Materials Conference, Denver, Colo., May 27-29, 1975; submitted Aug. 29, 1975; revision received July 14, 1976.

Index categories: Aeroelasticity and Hydroelasticity; VTOL Vibration; Structural Dynamic Analysis.

*Assistant Professor, School of Engineering and Applied Science, Mechanics and Structures Dept. Associate Fellow AIAA.

$T_{ddg}, \ldots T_f$ = flutter derivatives associated with the torsional equation, defined in Appendix B
U_{Y2}, U_{Z2} = relative velocity components of blade elastic axis, in the J_2, and K_2 directions
u, v, w = x, y, and z displacements of a point on the elastic axis of the blade
v_e, w_e = elastic part of the v, w displacements
x, y, z = rotating orthogonal coordinate system (Fig. 1)
X_2, Y_2, Z_2 = orthogonal coordinate system fixed at blade cross section, moving with the deformed blade oriented in I_2, J_2, K_2 directions, respectively (Fig. 2)
X_3, Y_3, Z_3 = orthogonal coordinate system fixed at blade cross section, moving with the deformed blade, oriented in the I_3, J_3, and K_3 directions, respectively
$x_0 = x - e_1$ = spanwise coordinate for elastic part of the blade, x_1 – same, dummy variable
x_A, $(\bar{x}_A = x_A/bR)$ = blade cross-sectional aerodynamic center offset from elastic axis, shown in Fig. 1. Positive for *A.C.* before *E.A.*
x_1, $(\bar{x}_1 = x_1/\ell)$ = blade cross-sectional mass center of gravity offset from the elastic axis (Fig. 1)

Greek symbols

β_P = preconing, inclination of the feathering axis with respect to the hub plane (Fig. 1)
γ = lock number $\gamma = (2\rho_A bR^5 a/I_b)$
γ_1 = first inplane bending mode shape
ϵ_D = symbolic quantity having the same order of magnitude as the displacements v and w
η_1 = first flapwise bending mode shape
η_{SF1}, η_{SL1} = viscous structural damping coefficients, in percent of critical damping, for first flap and lag mode, respectively
η, ζ = cross-sectional coordinates (Fig. 1) in the J_3 and K_3 directions, respectively
$\theta_G(\bar{x}_0)$ = total geometric pitch angle at a blade cross section, composed of built in twist and collective pitch
$\theta_B(\bar{x}_0)$ = built in twist, measured with respect to root chord
θ = collective pitch measured from x-y plane (hub plane)
θ_c = critical value of collective pitch setting at which linearized system becomes unstable, rad
λ = inflow ratio, induced velocity over disk, positive down, nondimensionalized with respect to ΩR
ρ_A = density of air
σ = blade solidity ratio (blade area/disk area)
ϕ = total elastic torsional deformation $(\phi = \phi_r + \phi_D)$
ϕ_r = root torsional elastic, deformation
ϕ_D = spanwise, distributed, torsional elastic deformation
ϕ_1 = first, coupled, root-torsional mode shape
ψ = azimuth angle of blade $(\psi = \Omega t)$ measured from straight aft position
$\bar{\omega}_{F1}$, $\bar{\omega}_{L1}$ = natural frequency of the first flap or lag mode (rotating)
$\bar{\omega}_{\phi 1}$ = natural frequency of the first torsional mode (rotating)
Ω = speed of rotation

Superscripts

$(\bar{\ })$ = nondimensionalized quantity, lengths associated with elastic bending, nondimensionalized with respect to ℓ; all others with respect to R; frequencies with respect to Ω; inertia properties with respect to I_b
$(\dot{\ })$ = differentiation with respect to ψ
$(\ )'$ = differentiation with respect to $\bar{x}_0$ $(= x_0/\ell)$

Introduction

In recent years the hingeless rotor, in which the blades are cantilevered to the hub, has become an increasingly attractive concept because of its mechanical simplicity of construction and favorable control characteristics. Although a number of quite successful hingeless rotored helicopters have been built and are in service, both in military and civilian applications, the hingeless rotor still has a stigma of aeroelastic problems associated with it. The purpose of the present paper is to illustrate that, when a reasonably complete model of the blade, such as developed in this study, is used, the aeroelastic problems appear to be milder than those apparent from previous studies.

A considerable amount of recent work[1-3] has been concentrated on the problem of aeroelastic modeling of a hingeless blade, in hovering flight. References 1 and 2 were devoted, primarily, to determining the effect of adding the torsional degree of freedom to a blade having only coupled flap-lag or flap-pitch degrees of freedom. The effect of precone and torsional flexibility has been studied extensively in Ref. 3. At the same time the sensitivity of the flutter boundaries to parameters of practical importance such as: blade cross-sectional aerodynamic center offset from elastic axis, blade cross-sectional mass center of gravity from elastic axis, structural damping, and the combined effect of these with precone has received only a very limited amount of attention.[4-6] Although Refs. 4 through 7 deal with some of these effects, these studies pertain to a particular helicopter configuration, and the analytical model from which the numerical values are generated is not presented. Therefore it seemed important to derive an analytical model for this aeroelastic problem, which would include all of the essential ingredients in a rational manner. The derivation of this mathematical model and its application to generate results indicating the sensitivity of the aeroelastic stability boundaries to the various parameters mentioned earlier is the main purpose of this study. Finally, results illustrating the effect of the exact nonlinear static equilibrium position and blade torsional modeling also are presented.

Equations of Motion

General

The present study is based upon a set of linearized coupled flap-lag-torsional equations of motion of a pretwisted cantilevered rotor blade. Both distributed torsional stiffness and root torsional flexibility are included in the formulation of the problem. The derivation itself is algebraically tedious and, thus, only a relatively brief description will be given in this paper.

The equations of motion first will be derived in partial differential, nonlinear forms, which subsequently are linearized. The derivation is based upon Refs. 1 and 8. The inertial and aerodynamic operators for this aeroelastic problem have been derived previously.[1] These operators are valid for moderately large blade deflections within the limitations of the assumption given in the following section. An excellent derivation of

the structural operator, for linear small deflection theory of rotating pretwisted beams has been presented by Houbolt and Brooks.[8] Fortunately, the approach used by Houbolt and Brooks is quite general, thus it has been modified in the present study to yield the appropriate structural operator for the case of moderately large deflections. Furthermore, in Ref. 9, it is shown that by a few minor modifications, the effect of root torsional flexibility can be included conveniently in the formulation of the problem.

Finally, it should be mentioned that various equations for the coupled flap-lag-torsional notion of a blade in hover are available in the literature.[1] Of these only the equations presented in Ref. 3 are similar to those of the present study, except that the effect of root torsion was not included in Ref. 3.

Basic Assumptions

The geometry of the problem is shown in Figs. 1 and 2. The following assumptions were used in deriving the equations of motion. 1) The blade is cantilevered at the hub, the feathering axis of the blade is preconed by an angle β_p. The angle β_p is small such that $\sin\beta_p \cong \beta_p$ and $\cos\beta_p \cong 1$, unless otherwise stated. 2) The blade can bend in two mutually perpendicular directions normal to the elastic axis of the blade, the boundary conditions for bending are those of a cantilevered beam. The torsional displacement of the blade consists of root torsion ϕ_r and distributed torsional flexibility ($\phi = \phi_r + \phi_D$). The torsional restraint at the root of the blade is represented by a torsional spring of stiffness k_ϕ. The axis of twist for root torsion coincides with the feathering axis whereas that for distributed torsion is the elastic axis. 3) The blade has an arbitrary amount of pretwist, which is assumed to be built-in about the elastic axis of the blade. 4) The blade cross section is symmetrical about the major principal axis. It has three distinct points, namely, the elastic axis (*E.A.*), aerodynamic center (*A.C.*), and center of gravity (*C.G.*). The *C.G.* = *E.A.* offset is denoted by x_I, and the *A.C.* = *E.A.* offset is denoted by x_A (see Fig. 1). 5) The deflections of the blade are moderately small so that terms of $O(\epsilon_D^2)$ can be neglected compared to one. Moderately large deflections have only a small effect on the tension in the blade since one of its end is free. 6) The resisting torque includes a St. Venant-type torsional term which is the same as would develop if the beam initially were untwisted together with a resisting moment due to pretwist. 7) Structural damping forces are assumed to be of a viscous type. 8) Two-dimensional quasisteady aerodynamic strip theory is used (i.e., Theodorsen's lift deficiency function $C(k) = 1$) and apparent mass effects, except those representing damping in pitch, are neglected. 9) Stall and compressibility effects are neglected. 10) Single blade analysis of an isolated rotor blade attached to an aircraft of infinite mass is used.

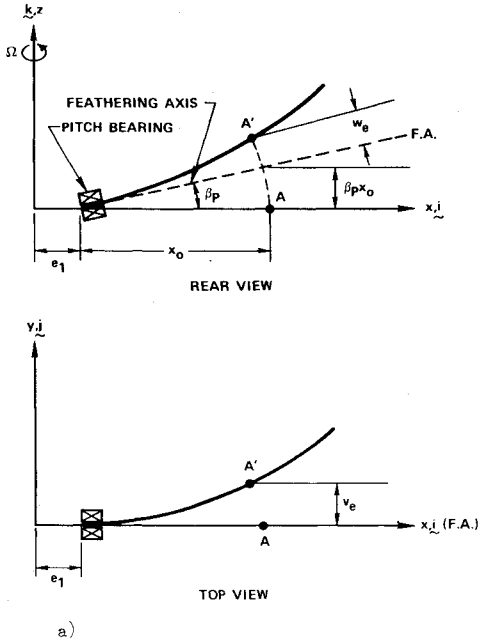

a)

Fig. 1a Deformed elastic axis for a cantilevered, preconed rotor blade.

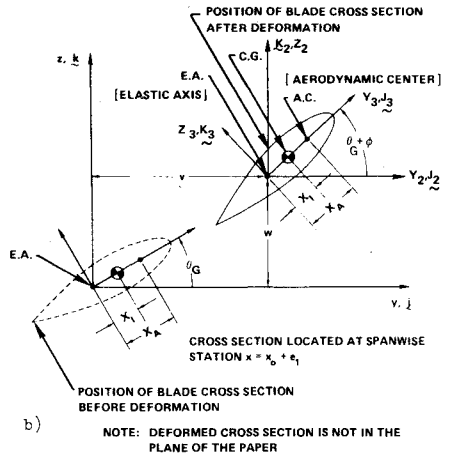

b)

Fig. 1b Blade model and positions of the cross section before and after the deformation.

The Ordering Scheme

The present study essentially is aimed at deriving first a set of nonlinear equations which subsequently will be linearized. In this process one encounters a considerable number of terms which are small and therefore negligible. In order to neglect the appropriate terms a rational ordering scheme is used which enables one to neglect terms in a systematic manner. In this scheme all of the important parameters of the problem are assigned orders of magnitude in terms of a typical displacement quantity ϵ_D thus,

$$\frac{v}{R} = O(\epsilon_D); \frac{w}{R} = O(\epsilon_D); \frac{x}{R} = O(1); \frac{\partial}{\partial x_0} = \frac{\partial}{\partial \psi} = O(1)$$

$$\theta = O(\epsilon_D^{1/2}); \phi = O(\epsilon_D); \lambda = O(\epsilon_D)$$

$$\beta_p = O(\ _D); C_{d0}/a = O(\epsilon_D^2)$$

$$\partial\theta_B/\partial x_0 = O(\epsilon_D); x_I/\ell = O(\epsilon_D^2); b = O(\epsilon_D)$$

$$k_0/\ell = O(\epsilon_D); \bar{x}_A = x_A/bR = O(1)$$

This ordering scheme together with assumption (7) of the preceding section means that terms of $O(\epsilon_D^2)$ are neglected

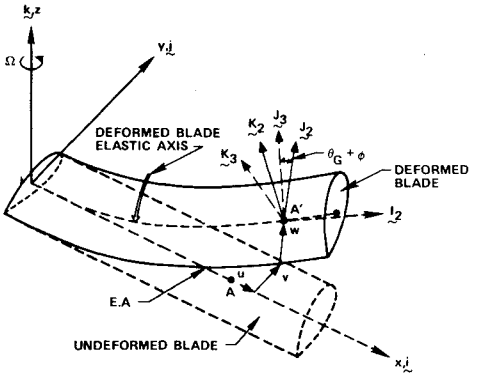

Fig. 2 Schematic representation of deformed and undeformed blade.

when compared to terms of $0(1)$ in the equations. Obviously the ordering scheme should be used with a certain degree of flexibility so as to enable one to retain certain higher-order terms even though they may appear negligible when considered strictly in the light of the ordering scheme. For example, in the torsional equation it can be shown that the leading terms are third-order terms; therefore, in this equation terms up to and including third-order terms have to be retained.

Brief Derivation of the Equations

Under the assumptions given previously a system of nonlinear partial differential equations for the coupled flap-lag-torsional motion of the blade is derived, with respect to a x,y, and z coordinate system rotating with the blade. The derivation of the inertia and aerodynamic operators of this aeroelastic problem follows essentially along the lines of Ref. 1 whereas the derivation of the structural operator will be outlined in the following.

The derivation of the structural operator for coupled bending and torsional motion of a pretwisted rotating beam has been presented by Houbolt and Brooks.[8] The introduction of moderately large deflection requires two modifications in the equations of Ref. 8. The first modification requires the derivation of a new nonlinear expression to replace the strain displacement equation, Eq. (A. 16) of Ref. 8. This is obtained by retaining second-order quantities associated with the elastic torsion in Eqs. (A. 3) of Ref. 8. The resulting strain displacement relation is given by

$$\epsilon_{xx}=\frac{T}{EA}+e_A\left[v_{e,xx}\cos(\theta_G+\phi)+w_{e,xx}\sin(\theta_G+\phi)\right]$$
$$-k_A^2\left(\theta_{B,x}\phi_{,x}+\frac{\phi_{,x}^2}{2}\right)+\left(\theta_{B,x}\phi_{,x}+\frac{\phi_{,x}^2}{2}\right)(\eta^2+\zeta^2)$$
$$-v_{e,xx}\left[\eta\cos(\theta_G+\phi)-\zeta\sin(\theta_G+\phi)\right]$$
$$-w_{e,xx}\left[\eta\sin(\theta_G+\phi)+\zeta\cos(\theta_G+\theta)\right] \tag{1}$$

where A is cross-sectional area of the blade.

The second modification to the Houbolt and Brooks equations[8] consists of using Eq. (1) in the calculation of the bending moments and the expressions for the torque. When using Eq. (1) to calculate these expressions, higher-order terms in the equations are retained, leading to nonlinear expression for the bending moments in the flap and lag directions and for the torque. These equations then are substituted into the equilibrium equations, Eqs. (17) of Ref. 8, leading to a set of nonlinear partial differential equations of equilibrium which are consistent with the ordering scheme described in the previous section. These partial nonlinear equations of equilibrium for the flap, lag, and torsional degrees of freedom, respectively, are given by

$$\frac{\partial^2}{\partial x_0^2}\left\{\left[(EI)_y+E_{c1}\right]\frac{\partial^2 v_e}{\partial x_0^2}+E_{c2}\frac{\partial^2 v_e}{\partial x_0^2}-EB_2\left[\frac{\partial\theta_B}{\partial x_0}\frac{\partial\phi}{\partial x_0}\right.\right.$$
$$\left.\left.+\frac{1}{2}\left(\frac{\partial\phi}{\partial x_0}\right)^2\right]\sin\theta_G+2E_{c2}\phi\frac{\partial^2 w_e}{\partial x_0^2}+E_{c3}\phi\frac{\partial^2 v_e}{\partial x_0^2}\right\}$$
$$-\frac{\partial}{\partial x_0}\left(T\frac{\partial w}{\partial x_0}\right)-\frac{\partial q_y}{\partial x_0}=P_z \tag{2}$$

$$\frac{\partial^2}{\partial x_0^2}\left\{E_{c2}\frac{\partial^2 w_e}{\partial x_0^2}+\left[(EI)_z-E_{c1}\right]\frac{\partial^2 v_e}{\partial x_0^2}-EB_2\left[\frac{\partial\theta_B}{\partial x_0}\frac{\partial\phi}{\partial x_0}\right.\right.$$
$$\left.\left.+\frac{1}{2}\left(\frac{\partial\phi}{\partial x_0}\right)^2\right]\cos\theta_G+E_{c3}\phi\frac{\partial^2 w_e}{\partial x_0^2}-2\phi E_{c2}\frac{\partial^2 v_e}{\partial x_0^2}\right\}$$
$$-\frac{\partial}{\partial x_0}\left(T\frac{\partial v}{\partial x_0}\right)+\frac{\partial q_z}{\partial x_0}=P_y \tag{3}$$

$$-\frac{\partial}{\partial x_0}\left\{GJ\frac{\partial\phi}{\partial x_0}+Tk_A^2\left(\frac{\partial\theta_B}{\partial x_0}+\frac{\partial\phi}{\partial x_0}\right)+EB_1\left(\frac{\partial\theta_B}{\partial x_0}\right)^2\frac{\partial\phi}{\partial x_0}\right.$$
$$+EB_1\frac{\partial\theta_B}{\partial x_0}\left(\frac{\partial\phi}{\partial x_0}\right)^2+\frac{EB_1}{2}\left[\frac{\partial\theta_B}{\partial x_0}\left(\frac{\partial\phi}{\partial x_0}\right)^2+\left(\frac{\partial\phi}{\partial x_0}\right)^3\right]$$
$$-EB_2\left(\frac{\partial\theta_B}{\partial x_0}+\frac{\partial\phi}{\partial x_0}\right)\left[\frac{\partial^2 v_e}{\partial x_0^2}\cos\theta_G+\frac{\partial^2 w_e}{\partial x_0^2}\sin\theta_G\right.$$
$$\left.\left.+\phi\frac{\partial^2 w_e}{\partial x_0^2}\cos\theta_G\right]\right\}+\left[(EI)_z-(EI)_y\right]\left\{\frac{\partial^2 v_e}{\partial x_0^2}\frac{\partial^2 w_e}{\partial x_0^2}(\cos^2\theta_G\right.$$
$$\left.-\sin^2\theta_G)+\left[\left(\frac{\partial^2 w_e}{\partial x_0^2}\right)^2-\left(\frac{\partial^2 v_e}{\partial x_0^2}\right)^2\right]\sin\theta_G\cos\theta_G\right\}$$
$$-EB_2\frac{\partial^2 w_e}{\partial x_0^2}\cos\theta_G\left[\frac{\partial\theta_B}{\partial x_0}\frac{\partial\phi}{\partial x_0}+\frac{1}{2}\left(\frac{\partial\phi}{\partial x_0}\right)^2\right]$$
$$+\left[(EI)_z-(EI)_y\right]\left[\left(\frac{\partial^2 w_e}{\partial x_0^2}\right)^2-\left(\frac{\partial^2 v_e}{\partial x_0^2}\right)^2\right]\phi\cos^2\theta_G$$
$$=q_x(x_0)+q_y\frac{\partial v}{\partial x_0}+q_z\frac{\partial w}{\partial x_0} \tag{4}$$

where for convenience $e_A=0$ in these equations and $(EI)_z$ and $(EI)_y$ are the bending rigidities about the major and minor neutral axes. In these equations T is the centrifugal tension in the blade.

The boundary conditions for this set of partial differential equations are

$$\text{at } x_0=0,\ v_e=w_e=\partial v_e/\partial x_0=\partial w_e/\partial x_0=0$$

whereas at $x_0=\ell$, the shears and moments are zero.

For the torsional equation the total torque at $x_0=\ell$ is zero, and at $x_0=0$, with the assumption $\theta_B'(0)=0$, one has

$$(GJ+Tk_A^2)(\partial\phi/\partial x_0)=k_\phi\phi(0) \tag{5}$$

Next it should be emphasized that the partial differential equations of equilibrium are valid for both root torsion and distributed torsion. A proof of this statement is outlined in Ref. 9.

Finally, the inertia and aerodynamic operators have been derived in Ref. 1 and can be written as

$$p_z=p_{zI}+L_{Z2}-g_{SF}\Omega\dot{w}_e \tag{6}$$
$$p_y=p_{yI}+L_{Y2}-g_{SL}\Omega\dot{v}_e \tag{7}$$
$$p_x=p_{xI}+L_x \tag{8}$$

In this study it was assumed that the aerodynamic load in the x direction $L_x=0$. The inertia loads are[1]

$$p_{xI}=-(\partial T/\partial x_0)=-m\Omega^2[-(x_0+e_I)-2\dot{v}] \tag{9}$$
$$p_{yI}=-m\Omega(\ddot{v}+2\dot{u}-v-x_I\cos\theta_G) \tag{10}$$
$$p_{zI}=-m\Omega^2\ddot{w} \tag{11}$$

The aerodynamic loads L_{z2} and L_{y2} in the z and y directions, respectively, are given by[1]

$$L_{Z2}=\rho_A abR[(\theta_G+\phi)U_{Y2}^2-U_{Z2}U_{Y2}$$
$$-(3/2-\bar{x}_A)U_{Y2}bR\Omega(\dot{\theta}_G+\dot{\phi})] \tag{12}$$

$$L_{Y2}=-\rho_A abR[(\theta_G+\phi)U_{Y2}U_{Z2}-U_{Z2}^2+(C_{d0}/a)U_{Y2}^2$$
$$+(1.5-\bar{x}_A)(U_{Z2})bR\Omega(\dot{\theta}_G+\dot{\phi})] \tag{13}$$

And the velocity components in the j_2 and K_2 directions are given by[1]

$$-U_{Y2}=\Omega[v+x_0+e_I] \tag{14}$$

$$-U_{Z2}=\Omega[R\lambda+\dot{w}+v(\partial w/\partial x_0)] \tag{15}$$

In a similar manner the distributed torque loadings are given by[1]

$$q_x = q_{xI}+q_{xA} \tag{16}$$

$$q_{xI} = m\Omega^2 x_I[-\ddot{w}\cos\theta_G+(\ddot{v}-v)(\sin\theta_G+\phi\cos\theta_G)]$$
$$-m(k_0^2+x_I^2)\Omega^2[\ddot{\phi}+(\sin\theta_G\cos\theta_G+\phi\cos 2\theta_G)] \tag{17}$$

$$q_{XA} = a\rho_A(bR)^2\{\bar{x}_A[U_{Y2}^2(\theta_G+\phi)-U_{Z2}U_{Y2}]$$
$$-(1-\bar{x}_A)(\bar{x}_A-0.5)bRU_{Y2}\Omega(\dot{\theta}_G+\dot{\phi})\} \tag{18}$$

$$q_{yI} = m\Omega^2 x_I(x_0+e_I)(\sin\theta_G+\ +\phi\cos\theta_G) \tag{19}$$

$$q_{zI} = -m\Omega^2 x_I(x_0+e_I+2\dot{v})\cos\theta_g \tag{20}$$

It can be shown that the effect of the aerodynamic torques q_{yA}, q_{zA} is negligible.

The last ingredient required to complete the formulation of the problem is the displacement field for a point on the elastic axis of the blade, given by

$$u=-\beta_p w_e-\frac{x_0}{2}\beta_p^2-\frac{1}{2}\int_0^{x_0}\left[\left(\frac{\partial w_e}{\partial x_I}\right)^2+\left(\frac{\partial v_e}{\partial x_I}\right)^2\right]dx_I \tag{21}$$

$$v=v_e \tag{22}$$

$$w=w_e\beta_p x_0 \tag{23}$$

Modal Equations

The system of general, coupled, partial differential equations of motion presented in the previous section is transformed into a system of ordinary nonlinear differential equations by using Galerkin's method to eliminate the spatial variable. In this process the elastic degrees of freedom in the problem are presented by the uncoupled free vibration modes of a rotating blade. The present study is restricted to the case of a single elastic mode representing each elastic degree of freedom. The modal representation of the elastic degrees of freedom is given by

$$w_e=\ell\eta_I(\bar{x}_0)g_I(\psi) \tag{24a}$$

$$v_e=-\ell\gamma_I(\bar{x}_0)h_I(\psi) \tag{24b}$$

$$\phi=\phi_I(\bar{x}_0)f_I(\psi) \tag{24c}$$

The ordinary nonlinear differential equations of motion for the case of $EB_I=EB_2=k_A=0$ are given by

$$\bar{M}_{FI}\ddot{g}_I+2\bar{\omega}_{FI}\bar{M}_{FI}\eta_{SFI}\dot{g}_I+\bar{M}_{FI}\bar{\omega}_{FI}^2 g_I=-\bar{E}^s g_I+\bar{E}^{cs}h_I$$
$$-2\bar{E}^2 f_I g_I+\bar{E}^3 f_I h_I+2P_{III}g_I\dot{h}_I-\beta_p\bar{B}^1$$
$$+2_p\bar{B}^3\dot{h}_I+\bar{x}_I\bar{B}^{19}+A_{FI} \tag{25}$$

$$\bar{M}_{LI}\ddot{h}_I+2\bar{\omega}_{LI}\bar{M}_{LI}\eta_{SLI}\dot{h}_I+\bar{\omega}_{LI}^2 M_{LI}h_I=\bar{E}^{cs}g_I+\bar{E}^s h_I$$
$$-2(\bar{M}_\eta)_{III}g_I\dot{g}_I-2\beta_p\bar{B}^{17}\dot{g}_I-2\bar{x}_I\bar{B}^{20}$$
$$+\bar{E}^4 f_I g_I+2\bar{E}^5 f_I h_I+A_{LI} \tag{26}$$

$$M_\phi\ddot{f}_I+\bar{\omega}_{\phi I}^2\bar{M}_I f_I=-\bar{x}_I[-\bar{B}^{30}\ddot{g}_I-(\ddot{h}_I-h_I)\bar{B}^{23}$$
$$-\bar{B}^{24}h_I-(\bar{B}^{25}\beta_p+\bar{B}^{26}g_I)]+(\bar{E}^4-\bar{E}^8)g_I h_I-\bar{E}^2 g_I^2$$
$$+\bar{E}^5 h_I^2-\bar{E}^6 g_I^2 f_I+E^7 h_I^2 f_I+A_{TI}-B^{28}(\bar{k}_0^2+\bar{x}_I^2) \tag{27}$$

where A_{FI}, A_{LI}, and A_{TI} are the generalized airloads in flap, lag, and torsion, respectively, given by

$$A_{FI}=\frac{\ell^2}{\Omega^2 I_b}\int_{\bar{A}}^{\bar{B}} L_{Z2}\eta_I d\bar{x}_0 \tag{28}$$

$$A_{LI}=-\frac{\ell^2}{\Omega^2 I_b}\int_{\bar{A}}^{\bar{B}} L_{Y2}\gamma_I d\bar{x}_0 \tag{29}$$

$$A_{TI}=\frac{\ell}{\Omega^2 I_b}\int_{\bar{A}}^{\bar{B}} q_{xA}\phi_I d\bar{x}_0 \tag{30}$$

Equations (25-27) are coupled ordinary nonlinear equations. These equations will be linearized about a suitable equilibrium position. In the past[1] this equilibrium position was taken usually as the approximate linear, steady state, equilibrium position of the blade in hover. However, in reality the exact equilibrium position should be obtained from the solution of the nonlinear algebraic system, Eqs. (32) given subsequently.

The process of linearization consists of expressing the elastic part of the displacement field as

$$w_e=\eta_I(g_I^\circ+\Delta g_I) \tag{31a}$$

$$v_e=-\gamma_I(h_I^\circ+\Delta h_I) \tag{31b}$$

$$\phi=\phi_I(f_I^\circ+\Delta f_I) \tag{31c}$$

Where the static equilibrium position is obtained from

$$[S]\begin{Bmatrix} g_I^\circ \\ h^\circ \\ f_I^\circ \end{Bmatrix}=\{C\}+\begin{Bmatrix} F_{SN}(g_I^\circ, h_I^\circ, f_I^\circ) \\ L_{SN}(g_I^\circ, h_I^\circ, f_I^\circ) \\ T_{SN}(g_I^\circ, f_I^\circ, f_I^\circ) \end{Bmatrix} \tag{32}$$

where F_{SN}, L_{SN}, and T_{SN} are lengthy general nonlinear expression of the static equilibrium position associated with the flap, lag, and torsional degrees of freedom, respectively. Detailed expressions for these functions can be found in Ref. 10.

The final linearized equations of motion are given by

$$\Delta\ddot{g}_I+\bar{g}_{DI}\Delta\dot{g}_I+(\bar{\omega}_{FI}^2+F_g)\Delta g_I=F_{dh}\Delta\dot{h}_I+F_h\Delta h_I$$
$$+F_{df}\Delta\dot{f}_I+F_f\Delta f_I \tag{33}$$

$$\Delta\ddot{h}_I+\bar{g}_{D2}\Delta\dot{h}_I+(\bar{\omega}_{LI}^2+L_h)\Delta h_I=L_{dg}\Delta\dot{g}_I+L_g\Delta g_I$$
$$+L_{df}\Delta\dot{f}_I+L_f\Delta f_I \tag{34}$$

$$\Delta\ddot{f}_I+\bar{g}_{D3}\Delta\dot{f}_I+(\bar{\omega}_\phi^2+T_f)\Delta f_I=T_{ddg}\Delta\ddot{g}_I+T_{dg}\dot{g}_I$$
$$+T_g\Delta g_I+T_{ddh}\Delta\ddot{h}_I+T_{dh}\Delta\dot{h}_I+T_h\Delta h_I \tag{35}$$

The various quantities used in these equations are described in Appendices A and B.

Static and Dynamic Stability Criteria

Static stability or divergence boundaries are related to the calculation of the static equilibrium position. In this paper two methods are employed for the calculation of the static equilibrium position: a) an *approximate* static equilibrium position is defined by the solution of Eqs. (32) with the

nonlinear terms F_{SN}, L_{SN}, T_{SN} neglected; b) an *exact* static equilibrium position is obtained from an exact solution of the nonlinear algebraic system, Eqs. (32), by using the Newton-Raphson method.[11]

Depending upon the approach used in calculating the static equilibrium position, three different divergence criteria can be formulated. The first is associated with the approximate static equilibrium position and is given by the condition[1] $\det([S])=0$. This, however, is not a very useful divergence criterion. An exact divergence criterion has been presented in Ref. 1. This criterion can be shown to be equivalent to the conditions under which the Newton-Raphson method of solution for Eqs. (32) fails to converge. When the exact nonlinear equilibrium position is calculated failure of the Newton-Raphson method is equivalent to the exact divergence boundary. When the approximate linear equilibrium values for g_l°, h_l°, f_l° are substituted into the exact divergence criterion[1] an *almost exact* divergence boundary is obtained.

Equations (33-35) can be rewritten in first-order state variable form. For this case the dynamic stability problem is reduced to the solution of the standard eigenvalue problem. The flutter boundaries of the system are obtained from the condition that the real part of one of the six eigenvalues associated with the system is equal to zero.[10]

Results and Discussion

Data for the Computation of the Stability Boundaries

In computing the numerical results a number of simplifying assumptions were made. Mass and stiffness properties along the span of the blade were assumed to be constant. For all cases constant inflow was assumed and the inflow was calculated from[1]

$$\lambda=(a\sigma/16)[(1+24\theta/a\sigma)^{1/2}-1] \tag{36}$$

Rotating mode shapes associated with the uncoupled free vibration problem for the flap, lag, and torsional degrees of freedom, respectively, were generated using Galerkin's method based upon five nonrotating cantilever-type mode shapes.† The various spanwise integrations were performed using seven-point Gaussian integration. The following common parameters were used in all of the calculations:

$$C_{d0}=0.01;\quad a=2\pi;\quad \sigma=0.08;\quad \bar{A}=0;\quad \bar{B}=1.0;$$

$$x_l=0;\quad e_l=0;\quad b=0.0313;\quad \gamma=8.0;\quad \bar{\omega}_{Fl}=1.14;$$

$$\bar{k}_0=k_0/\ell=0.02$$

Various other pertinent quantities are specified on the plots.

Finally, it should be pointed out that the mode shapes for flap and lag used in Ref. 9 were incorrect because in their computation a centrifugal tension integral taken from Yntema[12] expression for S_{qp}, $q\neq p$, p. 35) was used. This integral subsequently was found to be incorrect. For this reason the majority of the numerical results in Ref. 9 are incorrect; however, the conclusions remain unchanged. The error found in Ref. 12 indicates that its use should be avoided.

Results

The results obtained in this study are presented in Figs. 3-6. The rotating flap frequency used in calculating the results presented in this section is $\bar{\omega}_{Fl}=1.14029$ which is representative of typical hingeless blade configurations. The two torsional frequencies used can be considered to be representative of a blade with average and high torsional flexibility, respectively. Combining these flap and torsional frequencies with a wide range of lead-lag frequencies, as shown in the figures, covers most practical hingeless blade configurations.

†Unless otherwise stated distributed torsional flexibility was used.

The stability boundaries shown in this section consist, mostly, of two branches. A branch on the left-hand side of the plots between $0.2<\bar{\omega}_{Ll}<1.1$, which represents a flap-lag branch because the flutter frequency on this branch is close to the rotating lag frequency of the blade and the mechanism of the instability is identifiable as a flap-lag-type instability. The second branch of the stability boundary is associated mainly with the torsional degree of freedom and appears on the right-hand side of the figures, for values of $\bar{\omega}_{Ll}>1.1$. This branch can be either a divergence boundary or a flap-pitch, or lag-pitch-type instability. These occur at relatively high values of collective pitch.

The effect of the offset between the elastic axis and the aerodynamic center $\bar{x}_A$ is illustrated by Fig. 3. All stability boundaries presented in this figure are based upon the approximate equilibrium position, described in the previous section. As shown, the flap-lag branch of the stability boundaries is lowered by increasing $\bar{x}_A$ between 0 and 0.20 (corresponding to 10% of the chord) for the case of $\bar{\omega}_{\phi l}=6.1702$, as well as for $\bar{\omega}_{\phi l}=4.506$, however, for the case of $\bar{\omega}_{\phi l}=4.506$, the relatively small amount of torsional stiffness tolerates only smaller $\bar{x}_A$ offsets. For this reason the $\bar{\omega}_{\phi l}=4.506$ case is shown only for values of $0.0<\bar{x}_A<0.14$. More interesting is the effect of this offset on the boundaries associated with the torsional degree of freedom. First, it is important to note that the critical boundaries are the *almost exact* divergence boundaries defined in the previous section. For both torsional frequencies, with or without the $\bar{x}_A$ offset, the divergence boundaries are lower than the flap-pitch flutter boundaries. The $\bar{x}_A$ offset lowers these boundaries significantly for both torsional frequencies. In the case of the low torsional frequency, $\bar{\omega}_{\phi l}=4.506$, no stable equilibrium position exists with $\bar{x}_A=0.20$. It is important to point out that divergence, in rotary wing aeroelasticity, is a highly nonlinear phenomenon. Thus, divergence in rotary wing aeroelasticity is quite different from divergence in fixed wing aeroelasticity. The physical mechanism of the instability is provided by the combined torsional moments of drag forces acting through a moment arm provided by the steady-state flap deflection of the blade (destabilizing) and the lift forces acting through a moment arm provided by the steady lead-lag deflections of the blade (stabilizing), in addition to the moments due to the $\bar{x}_A$ offset. For this reason the divergence margins of the blade are lower for higher values of lead-lag frequency, because for these configurations the steady-state lead-lag deflections of the blade are smaller. This aspect of hingeless blade behavior already has been mentioned briefly in Ref. 1; however, the

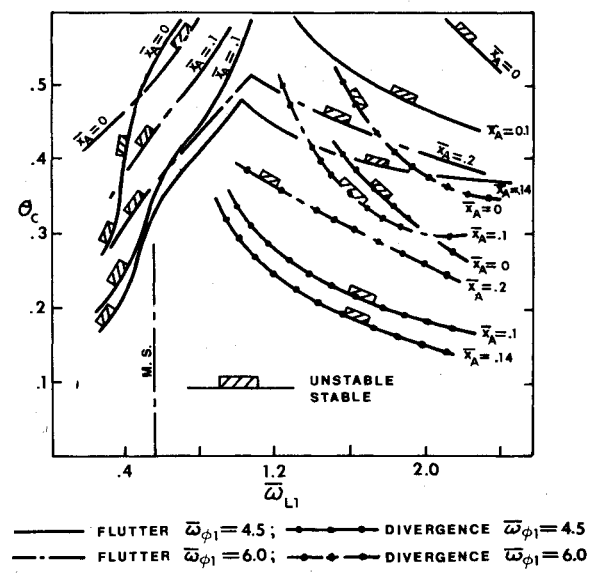

Fig. 3 Effect of offset between elastic axis and aerodynamic center for various torsional frequencies (for $\beta_p=0$ and $\eta_{SFI}=\eta_{SLI}=0$).

additional, detailed results presented here clearly emphasize this fundamental feature of rotary wing aeroelasticity.

The combined effect of precone and viscous-type structural damping is illustrated by Fig. 4. Again these results are based upon the approximate linear static equilibrium position. The main item of interest in this figure is the bubblelike region of instability occurring for low values of collective pitch θ. This instability occurs only in the presence of precone and it is a flap-lag-type instability. This instability also was obtained in Ref. 3. The unstable region decreases as the torsional stiffness $\bar{\omega}_{\phi 1}$ is increased from 4.5 to 6.0. The most important item, however, which has not been treated in Ref. 3, is the sensitivity of this unstable region to small amounts of viscous-type structural damping. For the case of low torsional frequency, $\bar{\omega}_{\phi 1}=4.5$, 0.25% of critical damping reduces the unstable region, while for $\bar{\omega}_{\phi 1}=6.0$ this small amount of damping completely elminates the unstable region, clearly indicating that the instability is a weak one. Additional results not included here indicate that this region is also quite sensitive to the type and number of the mode shapes used in the analysis. Finally, it should be mentioned that precone, as well as structural damping has only a minor effect on the other branches of the stability boundaries shown in Fig. 4; these branches are associated with high values of the collective pitch setting.

The results shown in the previous figures were based upon the approximate static equilibrium position and the distributed torsional representation of the blade stiffness. As stated in the previous section the equations presented are equally applicable to both root torsional modeling and distributed torsional modeling (or any combination of these two) for representing blade torsional deformations. Furthermore, stability boundaries also can be obtained easily when using the nonlinear exact static equilibrium position of the blade. The sensitivity of the stability boundaries to the assumptions made in modeling the blade torsional properties or in calculating the static equilibrium position of the blade is explored in Fig. 5. Two sets of stability boundaries are given in the figure, one for the root torsional representation of the blade and one for the case of distributed torsion. Furthermore, for each of these models two stability boundaries are presented: one based upon the approximate linear static equilibrium and one based upon the nonlinear exact static equilibrium position.

Comparing the flap-lag branches of the stability boundary it is clear that the boundaries with root torsion are considerably lower than with distributed torsion, this difference between the two boundaries is even more noticeable when the results are based upon the nonlinear static equilibrium position. It is also evident from these results that the inclusion of the nonlinear static equilibrium position is important in order to correctly represent physical blade behavior in the vicinity of the matched stiffness region, i.e., in this region the curves are much steeper when the nonlinear static equilibrium position is included. Significant differences are also apparent when comparing the flap-pitch branches of the stability boundaries presented. First, for the case of distributed torsion it is interesting to note that both the exact and almost exact divergence boundaries are lower than the flutter boundary; thus, for this representation divergence occurs before flutter. Furthermore, the exact divergence boundaries based upon the nonlinear static equilibrium position are about 20% lower than the most exact divergence boundaries. Even more interesting is the fact that for the case of

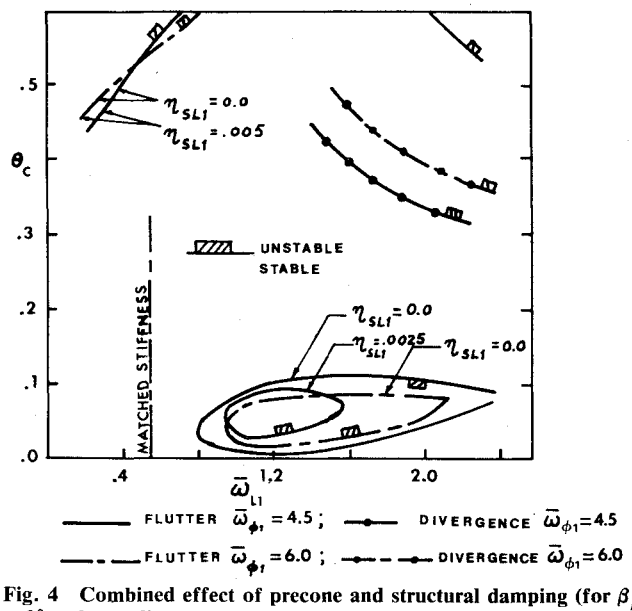

Fig. 4 Combined effect of precone and structural damping (for $\beta_p=3°$ and $\bar{x}_A=0$).

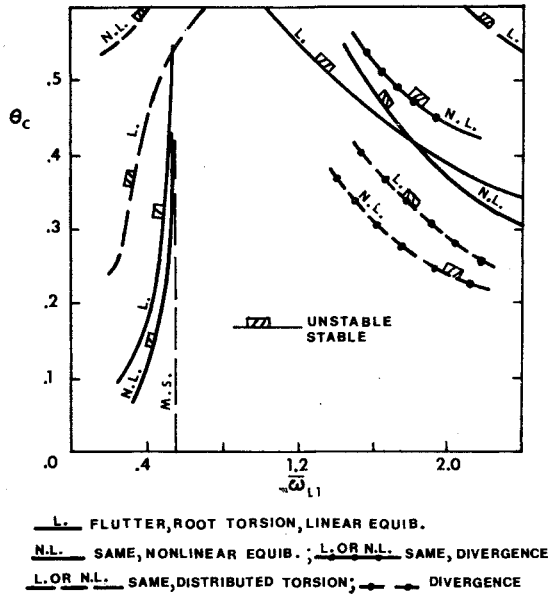

Fig. 5 Sensitivity of stability boundaries to blade torsional modeling and nonlinear static equilibrium position (with $\bar{x}_A=\beta_p=0$, and $\eta_{SFI}=\eta_{SLI}=0$).

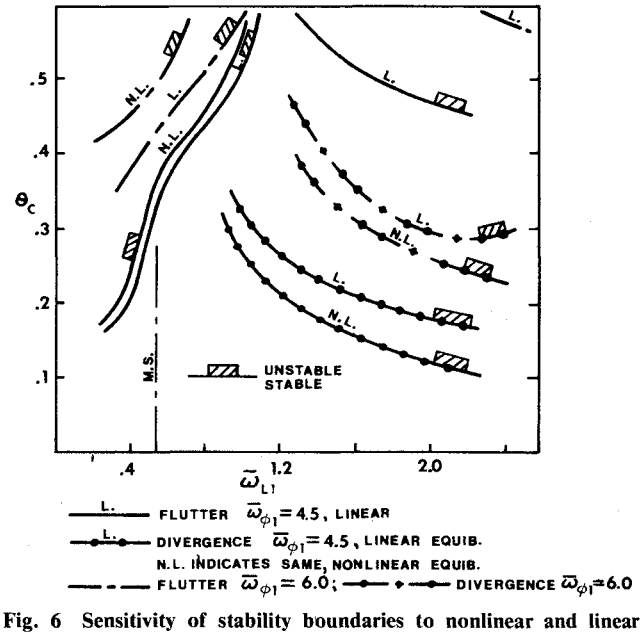

Fig. 6 Sensitivity of stability boundaries to nonlinear and linear static equilibrium position and x_A offsets (for $x_A=0.1$, $\beta_p=0$, and $\eta_{SFI}=\eta_{SLI}=0$).

root torsion the flutter boundaries in flap-pitch are lower than the divergence boundaries. Furthermore, the flutter boundaries based upon the approximate linear static equilibrium position are quite close to those obtained using the exact nonlinear static equilibrium position. Results are not presented here indicate[10] that divergence boundaries also can be sensitive to the number of modes used.

The combined effect of torsional flexibility, $\bar{x}_A$ offsets, and the sensitivity of the stability boundaries to the exact nonlinear static equilibrium position is illustrated further in Fig. 6. As shown, in the presence of an offset of 5% of blade chord ($\bar{x}_A = 0.10$) the difference between the flap-lag branches is not very sensitive to the type of equilibrium position used. It is important to note again that the divergence boundaries are most critical for the flap-pitch branch. Again the exact divergence boundaries based upon the nonlinear static equilibrium position are the most critical ones.

Conclusions

The major conclusions obtained from the present study are summarized as follows. They should be considered indicative of trends and their application to the design of a helicopter blade should be limited by the assumptions used.

1) Coupled flap-lag-torsional blade stability seems to be insensitive to small amounts of offset (1-2% of chord) between the aerodynamic center and the elastic axis. However values of $\bar{x}_A \geq 0.10$ (5% or more of chord) can lead to severe deterioration in both flutter and divergence boundaries.

2) Precone introduces coupling effects leading to a region of flap-lag-type instability at low collective pitch settings. This region is particularly sensitive to structural damping and torsional stiffness. For most cases small amounts of viscous-type structural damping (between 0.25-0.75% of critical) are sufficient to eliminate this unstable region for practical values of precone $\beta_p < 3°$, indicating that this a weak instability.

3) Retention of nonlinear terms in the calculation of the static equilibrium position substantially affects both flutter and divergence boundaries. The exact nonlinear divergence condition[1] is essential for the correct calculation of divergence boundaries for a hingeless blade.

4) Flutter and divergence boundaries based upon the root torsional representation of blade torsion can yield significantly different stability boundaries from those obtained when the distributed torsional representation of blade torsional flexibility is used.

Appendix A: Definition of the Generalized Masses, Aerodynamics, and Various Structural Integrals

The definition of the quantities $\bar{M}_{FI}$, $\bar{M}_{LI}$, $\bar{P}_{III}$, $(\bar{M}_\eta)_{III}$, $\bar{B}^1$, $\bar{B}^3$, $\bar{B}^7$, F^2, F^8, F^{10}, F^{11}, L^2, L^8, L^{14}, L^4 can be found in Ref. 2.

Additional generalized mass quantities are defined as follows

$$\bar{B}^{19} = \ell^3 \int_0^1 m\eta_1 \sin\theta_G \frac{d\bar{x}_0}{I_b} \tag{A1a}$$

$$\bar{B}^{20} = \ell^3 \int_0^1 m\gamma_1 \cos\theta_G \frac{d\bar{x}_0}{I_b} \tag{A1b}$$

$$\bar{B}^{21} = \ell^3 \int_0^1 m\gamma_1\gamma_1' \cos\theta_G \frac{d\bar{x}_0}{I_b} \tag{A1c}$$

$$\bar{B}^{23} = \ell^3 \int_0^1 m\gamma_1\phi_1 \sin\theta_G \frac{d\bar{x}_0}{I_b} \tag{A1d}$$

$$\bar{B}^{24} = \ell^3 \int_0^1 m(\bar{x}_0 + \bar{e}_1) \sin\theta_G \gamma_1'\phi_1 \frac{d\bar{x}_0}{I_b} \tag{A1e}$$

$$\bar{B}^{25} = \ell^3 \int_0^1 m(\bar{x}_0 + \bar{e}_1) \cos\theta_G \phi_1 \frac{d\bar{x}_0}{I_b} \tag{A1f}$$

$$\bar{B}^{26} = \ell^3 \int_0^1 m(\bar{x}_0 + \bar{e}_1) \cos\theta_G \eta_1'\phi_1 \frac{d\bar{x}_0}{I_b} \tag{A1g}$$

$$\bar{B}^{28} = \ell^3 \int_0^1 m\phi_1 \sin\theta_G \cos\theta_G \frac{d\bar{x}_0}{I_b} \tag{A1h}$$

$$\bar{B}^{29} = \ell^3 \int_0^1 m\phi_1^2 \cos^2\theta_G \frac{d\bar{x}_0}{I_b} \tag{A1i}$$

$$\bar{B}^{30} = \ell^3 \int_0^1 m\eta_1\phi_1 \cos 2\,\theta_G \frac{d\bar{x}_0}{I_b} \tag{A1j}$$

The additional aerodynamic integrals, denoted by F^i, L^i, and T^i, respectively, for the flap, lag, and torsional equation, required for the present study are (with $\bar{x} = \bar{x}_0 + \bar{e}_1$)

$$F_\theta^1 = \int_{\bar{A}}^{\bar{B}} \theta_G(\bar{x}_0)\bar{x}^2\eta_1 d\bar{x}_0 \quad ; \quad F_\phi^1 = \int_{\bar{A}}^{\bar{B}} \phi_1\eta_1\bar{x}^2 d\bar{x}_0 \tag{A2a}$$

$$F^{10} = \int_{\bar{A}}^{\bar{B}} \bar{x}_0\eta_1\gamma_1\theta_G d\bar{x}_0 \quad ; \quad F_\phi^{10} = \int_{\bar{A}}^{\bar{B}} \phi_1\bar{x}_0\eta_1\gamma_1 d\bar{x}_0 \tag{A2b}$$

$$F^{25} = \int_{\bar{A}}^{\bar{B}} \bar{x}_0\eta_1\gamma_1\theta_G d\bar{x}_0 \quad ; \quad F_\phi^2 = \int_{\bar{A}}^{\bar{B}} \phi_1\eta_1\bar{x} d\bar{x}_0 \tag{A2c}$$

$$L_\theta^1 = \int_{\bar{A}}^{\bar{B}} \bar{x}\theta_G(\bar{x}_0)\gamma_1 d\bar{x}_0 \qquad L_\phi^1 = \int_{\bar{A}}^{\bar{B}} \phi_1\gamma_1\bar{x} d\bar{x}_0 \tag{A2d}$$

$$L_\theta^7 = \int_{\bar{A}}^{\bar{B}} \bar{x}\theta_G\eta_1\gamma_1 d\bar{x}_0 \quad ; \quad L_\phi^7 = \int_{\bar{A}}^{\bar{B}} \phi_1\bar{x}\eta_1\gamma_1 d\bar{x}_0 \tag{A2e}$$

$$L_\theta^{13} = \int_{\bar{A}}^{\bar{B}} \theta_G\gamma_1^2 d\bar{x}_0 \quad ; \quad L_\theta^{14} = \int_{\bar{A}}^{\bar{B}} \gamma_1^2\bar{x}\theta_G d\bar{x}_0 \tag{A2f}$$

$$L_\theta^{25} = \int_{\bar{A}}^{\bar{B}} \gamma_1^2\eta_1'\bar{x}\theta_G d\bar{x}_0 \tag{A2g}$$

$$T_\theta^1 = \int_{\bar{A}}^{\bar{B}} \phi_1\bar{x}\theta_G d\bar{x}_0 \quad ; \quad T_\phi^1 = \int_{b\bar{a}}^{\bar{B}} \phi_1^2\bar{x}^2 d\bar{x}_0 \tag{A2h}$$

$$T_\phi^2 = \int_{\bar{A}}^{\bar{B}} \phi_1\bar{x} d\bar{x}_0 \quad ; \quad T^3 = \int_{\bar{A}}^{\bar{B}} \gamma_1\phi_1\theta_G\bar{x} d\bar{x}_0 \tag{A2i}$$

$$T^4 = \int_{\bar{A}}^{\bar{B}} \gamma_1\phi_1^2\bar{x} d\bar{x}_0 \quad ; \quad T^5 = \int_{\bar{A}}^{\bar{B}} \gamma_1\phi_1 d\bar{x}_0 \tag{A2j}$$

$$T^6 = \int_{\bar{A}}^{\bar{B}} \eta_1\gamma_1\phi_1 d\bar{x}_0 \quad ; \quad T^7 = \int_{\bar{A}}^{\bar{B}} \bar{x}\gamma_1\phi_1 d\bar{x}_0 \tag{A2k}$$

$$T^8 = \int_{\bar{A}}^{\bar{B}} \bar{x}\phi_1\gamma_1\eta_1' d\bar{x}_0 \quad ; \quad T^3 = \int_{\bar{A}}^{\bar{B}} \phi_1\gamma_1^2\theta_G d\bar{x}_0 \tag{A2l}$$

$$T^{10} = \int_{\bar{A}}^{\bar{B}} \phi_1^2\gamma_1^2 d\bar{x}_0 \quad ; \quad T^{11} = \int_{\bar{A}}^{\bar{B}} \phi_1\gamma_1^2 d\bar{x}_0 \tag{A2m}$$

$$T^{12} = \int_{\bar{A}}^{\bar{B}} \gamma_1^2\phi_1\eta_1' d\bar{x}_0 \quad ; \quad T^{13} = \int_{\bar{A}}^{\bar{B}} \phi_1^2\gamma_1 d\bar{x}_0 \tag{A2n}$$

$$T^{14} = \int_{\bar{A}}^{\bar{B}} \phi_1^2\bar{x} d\bar{x}_0 \tag{A2o}$$

Various structural integrals are defined:

$$E_{c1} = [(EI)_z - (EI)_y]\sin^2\theta_G \tag{A3a}$$

$$E_{c2} = [(EI)_z - (EI)_y]\sin\theta_G\cos\theta_G \tag{A3b}$$

$$E_{c3}=[(EI)_z-(EI)_y]\cos^2\theta_G \tag{A3c}$$

$$\bar{E}^s=\int_0^1 E_{c1}\eta_1''^2\frac{d\bar{x}_0}{\Omega^2\ell I_b}=\bar{\bar{E}}^{cs} \tag{A3d}$$

$$\bar{E}^{cs}=\int_0^1 E_{c2}\gamma_1''\eta_1''\frac{d\bar{x}_0}{\Omega^2\ell I_b}=\bar{\bar{E}}^{cs} \tag{A3e}$$

$$\bar{\bar{E}}^s=\int_0^1 E_{c1}(\gamma_1'')^2\frac{d\bar{x}_0}{\Omega^2\ell I_b} \tag{A3f}$$

$$E^2=\int_0^1 E_{c2\,1}(\eta_1'')^2\frac{d\bar{x}_0}{I_b\Omega^2\ell} \tag{A3g}$$

$$\bar{E}^3=\int_0^1 E_{c3}\phi_1\gamma_1''\eta_1''\frac{d\bar{x}_0}{\Omega^2\ell I_b}=\bar{E}^4 \tag{A3h}$$

$$\bar{E}^5=\int_0^1 E_{c2}\phi_1(\gamma_1'')^2\frac{d\bar{x}_0}{I_B\Omega^2\ell} \tag{A3i}$$

$$\bar{E}^6=\int_0^1 E_{c3}\phi_1^2(\eta_1'')^2\frac{d\bar{x}_0}{\Omega^2\ell I_b} \tag{A3j}$$

$$\bar{E}^7=\int_0^1 E_{c3}\phi_1^2(\gamma_1'')^2\frac{d\bar{x}_0}{\Omega^2\ell I_b} \tag{A3k}$$

$$\bar{E}^8=\int_0^1 E_{c1}\eta_1''\gamma_1''\frac{d\bar{x}_0}{\Omega^2\ell I_b} \tag{A3l}$$

Various additional quantities are given as:

$$2\bar{\omega}_{F1}\bar{M}_{F1}\eta_{SF1}=\ell^3 g_{SF}\int_0^1 \eta_1^2\frac{d\bar{x}_0}{\Omega I_b} \tag{A4}$$

$$2\bar{\omega}_{L1}\bar{M}_{L1}\eta_{SL1}=\ell^3 g_{SL}\int_0^1 \gamma_1^2\frac{d\bar{x}_0}{\Omega I_b} \tag{A5}$$

$$M_{\phi 1}=\ell^3(\bar{x}_0^2+\bar{k}_0^2)\int_0^1 m\,\phi_1^2\frac{d\bar{x}_0}{I_b}=\frac{I_{\phi 1}}{I_b} \tag{A6}$$

$$\bar{\omega}_{\phi 1}^2=\Big[\int_0^1 m(\bar{k}_0^2+\bar{x}_1^2)\phi_1^2\cos 2\theta\,d\bar{x}_0+\int_0^1 [GJ+T\bar{k}_A^2\ell^2+EB_1(\theta')^2/\ell^2]\phi_1'^2\frac{d\bar{x}_0}{\ell}+k_\phi\phi_1^2(0)\Big]\Big/\Big[\Omega^2\ell^3\int_0^1 m(\bar{k}_0^2+\bar{x}_1^2)\phi_1^2 d\bar{x}_0\Big] \tag{A7}$$

$$EB_1=\int_{CS}\int(\eta^2+\zeta^2)(\eta^2+\zeta^2-k_A^2)E\,d\eta\,d\zeta \tag{A8a}$$

$$EB_2=\int_{CS}\int(\eta^2+\zeta^2)(\eta-e_A)E\,d\eta\,d\zeta \tag{A8b}$$

where η, ζ are local coordinates in the cross section in the J_3 and K_3 directions.

Appendix B: Flutter Derivatives and Quantities Required for the Calculation of the Static Equilibrium

The elements of $[S]$ and $\{C\}$ matrices are given as:

$$S_{11}=\bar{\omega}_{F1}^2\bar{M}_{F1}+\bar{E}^s\quad;\quad S_{12}=-\bar{E}^{cs}-\frac{\gamma}{2}\Big(\frac{\ell}{R}\Big)^3\beta_P F^{10}$$

$$S_{13}=-\frac{\gamma}{2}\Big(\frac{\ell}{R}\Big)^2 F_\phi^1\quad;\quad S_{21}=-\bar{\bar{E}}^{cs}$$

$$S_{22}=\bar{M}_{L1}\bar{\omega}_{L1}^2-\bar{\bar{E}}^s+\frac{\gamma}{2}\Big(\frac{\ell}{R}\Big)^3 L_\theta^{14}\beta_p;\quad S_{23}=-\frac{\gamma}{2}\Big(\frac{\ell}{R}\Big)^2 L_\phi^1$$

$$S_{31}=\bar{x}_1\bar{B}^{26};\quad S_{32}=\bar{x}_1(\bar{B}^{24}-\bar{B}^{23})-\frac{\gamma}{2}\Big(\frac{\ell}{R}\Big)^2 b\bar{x}_A\beta_P T^7$$

$$S_{33}=\bar{M}_{\phi 1}\bar{\omega}_{\phi 1}^2-\frac{\gamma}{2}\Big(\frac{\ell}{R}\Big)b\bar{x}_A T_\phi^1$$

$$C_1=\frac{\gamma}{2}\Big(\frac{\ell}{R}\Big)^2(F_\theta^1-\lambda F^2)-\beta_P\bar{B}^1+\bar{x}_1\bar{B}^{19}$$

$$C_2=\frac{\gamma}{2}\Big(\frac{\ell}{R}\Big)^2\Big(L_\theta^1\lambda-\lambda^2L^2+\frac{C_{d0}}{a}L^4\Big)-2\bar{x}_1\bar{B}^{20}$$

$$C_3=\frac{\gamma}{2}\Big(\frac{\ell}{R}\Big)b\bar{x}_A(T_\theta^1-T_\phi^2\lambda)-\bar{B}^{28}(\bar{x}_1^2+\bar{k}_0^2)-x_1\bar{B}^{25}\beta_P$$

The flutter derivatives are given by

$$\bar{g}_{D1}=2\bar{\omega}_{F1}\eta_{SF1}+(\gamma/2)(\ell/R)^3F^8/\bar{M}_{F1}$$

$$F_g=[\bar{E}^s+2\bar{E}^2f_1^\circ-(\gamma/R)^3F^{25}h_1^\circ]/\bar{M}_{F1}$$

$$F_h=[(\bar{E}^{cs}+\bar{E}^3f_1^\circ)+(\gamma/2)(\ell/R)^3(F^{10}\beta_p+F^{25}g_1^\circ)]/\bar{M}_{F1}$$

$$F_{df}=(1.5-\bar{x}_A)bF_\phi^2(\gamma/2)(\ell/R)^2/\bar{M}_{F1}$$

$$F_f=[-2E^2g_1^\circ+\bar{E}^3h_1^\circ+(\gamma/2)(\ell/R)^2F_\phi^1]\%\bar{M}_{F1}$$

$$F_{ddf}=F_{ddh}=0$$

$$\bar{g}_{D2}=2\bar{\omega}_{L1}^2\eta_{SL1}+[(\gamma/2)(\ell/R)^3(L_\theta^{13}\lambda+2C_{d0}L^{14}/a)]/\bar{M}_{L1}$$

$$L_h=-(\bar{\bar{E}}^s+2\bar{E}^5f_1^\circ)/\bar{M}_{L1}+(\gamma/2)(\ell/R)^3[L_\theta^{14}\beta_p+L_\theta^{25}g_1^\circ]/\bar{M}_{L1}$$

$$L_{dg}=\{-2[\beta_P\bar{B}^7+(\bar{M}_\eta)_{111}g_1^\circ]+(\gamma/2)(\ell/R)^3(L_\theta^7+L_\phi^7f_1-2\lambda L^8)\}/\bar{M}_{L1}$$

$$L_g=(\bar{\bar{E}}_{cs}+E^4f_1^\circ)/\bar{M}_{L1}-(\gamma/2)(\ell/R)^3h_1^\circ L_\theta^{25}/\bar{M}_{L1}$$

$$L_f=[\bar{E}^4g_1^\circ+2\bar{E}^5h_1^\circ+(\gamma/2)(\ell/R)^2L_\phi^1\lambda]/\bar{M}_{L1}$$

$$\bar{g}_{D3}=[-(1-\bar{x}_A)(\bar{x}_A-0.5)(\gamma/2)(\ell/R)b^2T^{14}]/\bar{M}_{\phi 1}$$

$$T_f=[\bar{E}^6(g_1^\circ)^2-\bar{E}^7(h_1^\circ)^2-(\gamma/2)(\ell/R)b\bar{x}_AT_\phi^1]/\bar{M}_{\phi 1}$$

$$T_{ddg}=-\bar{x}_1\bar{B}^{30}/\bar{M}_{\phi 1}$$

$$T_{dg}=-(\gamma/2)(\ell/R)^2b\bar{x}_AF_\phi^2/\bar{M}_{\phi 1}$$

$$T_g=[+\bar{x}_1\bar{B}^{26}+(\bar{E}^4-\bar{E}^8)h_1^\circ-E^22g_1^\circ-\bar{E}^62g_1^\circ f_1^\circ+(\gamma/2)(\ell/R)^2b\bar{x}_Ah_1^\circ T^8]/\bar{M}_{\phi 1}$$

$$T_{ddh}=-\bar{x}_1\bar{B}^{23}/\bar{M}_{\phi 1}$$

$$T_{dh}=[-\gamma(\ell/R)^2b\bar{x}_A(T^3+T^4f_1^\circ)+(\gamma/2)(\ell/R)^2b\bar{x}_A\lambda T^5+(\gamma/2)(\ell/R)^3b\bar{x}_A(h_1^\circ\beta_PT^{11}+h_1^\circ T^{12}g_1^\circ)]/\bar{M}_{\phi 1}$$

$$T_h=[\bar{x}_1(\bar{B}^{23}-\bar{B}^{24})+(\bar{E}^4-\bar{E}^8)g_1^\circ+\bar{E}^52h_1^\circ+\bar{E}^72f_1^\circ h_1^\circ+(\gamma/2)(\ell/R)^2b\bar{x}_A(\beta_PT^7+g_1^\circ T^8)]/\bar{M}_{\phi 1}$$

Acknowledgment

This work was supported by the Langley Directorate, U.S. Army Air Mobility R&D Lab., and NASA Langley Research

Center, Hampton, Va., under NASA NGR 05-007-414. The constructive suggestions of the project monitor C.E. Hammond are gratefully acknowledged. The fruitful discussions with my students R. Powers, and J. Shamie and their help in generating some of the results for this paper are gratefully acknowledged.

References

[1]Friedmann, P. and Tong, P., "Dynamic Nonlinear Elastic Stability of Helicopter Rotor Blades in Hover and in Forward Flight," NASA CR-114485, May 1972; also MIT ASRL 166-3.

[2]Friedmann, P., "Aeroelastic Instabilities of Hingeless Helicopter Blades," *Journal of Aircraft*, Vol. 10, Oct. 1973, pp. 623-631.

[3]Hodges, D. H. and Ormiston, R. A., "Stability of Elastic Bending and Torsion of Uniform Cantilevered Rotor Blades in Hover," AIAA Paper 73-405, Williamsburg, Va., 1973.

[4]Huber, H. B., "Effect of Torsion-Flap-Lag Coupling on Hingeless Rotor Stability," *29th Annual Forum of the American Helicopter Society*, May 1973.

[5]Anderson, W. D., "Investigation of Reactionless Mode Stability Characteristics of a Stiff Inplane Hingeless Rotor System," *29th Annual Forum of the American Helicopter Society*, May 1973.

[6]Burkam, J. E. and Miao, W., "Exploration of Aeroelastic Stability Boundaries with a Soft-in-Plane Hingeless-Rotor Model," *Journal of the American Helicopter Society*, Vol. 17, Oct. 1972, pp. 27-35.

[7]Friedmann, P. and Tong, P., "Nonlinear Flap-Lag Dynamics of Hingeless Helicopter Blades in Hover and in Forward Flight," *Journal of Sound and Vibration*, Vol. 30 (1), 1973, pp. 9-31.

[8]Houbolt, J. C. and Brooks, G. W., "Differential Equations of Motion for Combined Flapwise Bending, Chordwise Bending, and Torsion of Twisted Nonuniform Rotor Blades," NACA Rept. 1346, 1958.

[9]Friedmann, P., "Influence of Structural Damping, Preconing, Offsets and Large Deflections on the Flap-Lag-Torsional Stability of a Cantilevered Rotor Blade," AIAA Paper 75-780, Denver, Colo., 1975.

[10]Powers, R., "A Study of Several Approximation Concepts in Rotary-Wing Aeroelasticity," M.S. Thesis, June 1976, Mechanics and Structures Dept., University of California, Los Angeles.

[11]Carnahan, B., Luther, H. A., and Wilkes, J. O., *Applied Numerical Methods*, Wiley, New York, 1969, pp. 319-320.

[12]Yntema, R. T., "Simplified Procedures and Charts for the Rapid Estimation of Bending Frequencies of Rotating Beams," NACA TN 3459, 1955.